Simultaneous Chronoamperometry and Piezoelectric Microgravimetry Determination of Nitroaromatic Explosives Using Molecularly Imprinted Thiophene Polymers

ARTICLE *in* ANALYTICAL CHEMISTRY · AUGUST 2013

Impact Factor: 5.64 · DOI: 10.1021/ac4017677 · Source: PubMed

7 AUTHORS, INCLUDING:

Tan-Phat Huynh
Technion - Israel Institute of Technology
14 PUBLICATIONS **82** CITATIONS
SEE PROFILE

Janusz W. Sobczak
Polish Academy of Sciences
197 PUBLICATIONS **2,642** CITATIONS
SEE PROFILE

Volodymyr V Nesterov
New Mexico Highlands University
322 PUBLICATIONS **1,341** CITATIONS
SEE PROFILE

analytical chemistry

Article

pubs.acs.org/ac

Simultaneous Chronoamperometry and Piezoelectric Microgravimetry Determination of Nitroaromatic Explosives Using Molecularly Imprinted Thiophene Polymers

Tan-Phat Huynh,[†,‡] Marta Sosnowska,[†,‡] Janusz W. Sobczak,[†] Chandra B. KC,[‡] Vladimir N. Nesterov,[‡] Francis D'Souza,*[,‡] and Wlodzimierz Kutner*[,†,§]

[†]Department of Physical Chemistry of Supramolecular Complexes, Institute of Physical Chemistry, Polish Academy of Sciences (IPC PAS), Kasprzaka 44/52, 01-224 Warsaw, Poland

[‡]Department of Chemistry, University of North Texas, 1155 Union Circle No. 305070, Denton, Texas 76203-5017, United States

[§]Faculty of Mathematics and Natural Sciences, School of Science, Cardinal Stefan Wyszynski University in Warsaw, Wóycickiego 1/3, 01-815 Warsaw, Poland

Supporting Information

ABSTRACT: Thin films of conducting molecularly imprinted polymers (MIPs) were prepared for simultaneous chronoamperometry (CA) and piezoelectric microgravimetry (PM) determination of several explosive nitroaromatic compounds (NTs) including 2,4,6-trinitrophenol (TNP), 2,4,6-trinitrotoluene (TNT), 1,3,5-trinitrobenzene (TNB), and 2,4-dinitrotoluene (DNT). For that, the bis(2,2′-bithienyl)-(4-aminophenyl)methane **1** functional monomer allowing for $\pi-\pi$ stacking recognition of the NTs was designed and synthesized. Both theoretical DFT calculations at the M062X/3-21G* level and experimental fluorescence titrations indicated the 1:1 stoichiometry of the **1** and NT prepolymerization complexes formed in solutions. The NT-templated MIP (MIP-NT) films were deposited by potentiodynamic electropolymerization on the Au-coated quartz crystal resonators (Au-QCRs) from solutions of **1** and each of the NT templates at the **1**-to-NT mole ratio of 1:1. For sensing application, the NTs were extracted from the MIP-NT films. Completeness of the extraction was confirmed by the presence and absence before and after extraction, respectively, of both the XPS peak of the N 1s electrons of the NT nitro groups and the DPV peak of electroreduction of the NTs for the MIP-NT. Ultimately, the recognition signal was transduced to the analytical signal of simultaneous changes of CA cathodic current and PM resonant frequency. The limit of detection (LOD) for NTs was in the range of hundreds and tens micromolar for CA and PM, respectively. Moreover, selectivity with respect to common interferences of the chemosensors was in the range 2.1−4.8, as determined by molecular cross-imprinting.

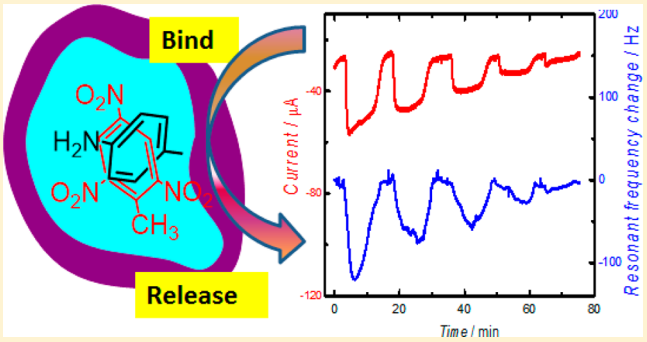

Nitro compounds are the most common explosives used not only by the military (bombs, mines, grenades) but also for civil engineering (blasting devices, propellants, fireworks, etc.). For that, over 100 different nitro compounds are used. Among them, nitro-substituted hydrocarbons consist of one of the largest groups. In this group, the nitro substituents are directly attached to the carbon atoms of alkane chain or an aromatic ring of the hydrocarbon. Importantly, the more nitro groups on the molecule of the explosive, the higher the energy of detonation is. Therefore, nitroaromatic compounds (NTs) carrying three nitro groups per molecule, such as 2,4,6-trinitrotoluene (TNT), 1,3,5-trinitrobenzene (TNB), and 2,4,6-trinitrophenol, i.e., picric acid (TNP) (Scheme 1), are among those most highly explosive. Moreover, the toxic effect of these explosives caused by their contamination (in the micromolar range) of soil, water, or air poses a serious threat to people.[1−4]

Scheme 1. Structural Formulas of Four Common Explosive Nitroaromatic Compounds[a]

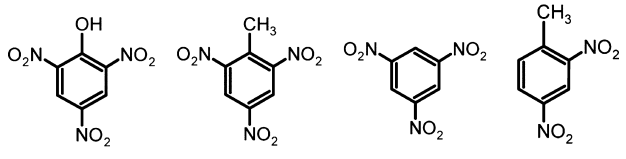

[a]TNP, 2,4,6-trinitrophenol (picric acid); TNT, 2,4,6-trinitrotoluene; TNB, 1,3,5-trinitrobenzene; DNT, 2,4-dinitrotoluene.

Received: June 12, 2013
Accepted: July 25, 2013
Published: July 25, 2013

Hence, low-cost, high-sensitivity, and high-selectivity sensors for detection and determination of NTs are in demand.[5,6]

Due to electroreductive properties of NTs, many electrochemical sensors were fabricated for determination of NTs in water.[7] Sensitivity and selectivity of NT sensors is improved if molecularly imprinted polymers (MIPs) are used as their sensing units. This is because size, shape, and orientation of recognition sites of the cavities imprinted in MIPs accurately match up those of the molecules of target analytes.[8−11] For instance, a recognition signal of the MIP film complexation of butanethiol and 2,4-dinitrotoluene (DNT) or TNT in ethanol was transduced to the charge-transfer resistance signal of the $K_4Fe(CN)_6$ redox probe.[12] However, the limit of detection (LOD) of this chemical sensor was high (∼40 μM) because interaction of the NT compounds and butanethiol was weak in a polar protic solvent such as ethanol used for formation of a prepolymerizational complex. But this LOD was brought to as low value as 13 nM TNT with the use of differential pulse voltammetry (DPV) transduction and by replacing this protic solvent by that aprotic acetonitrile and butanethiol by self-assembled 1-dodecanethiol monolayer.[13]

Moreover, MIP-fluorescence chemosensors were fabricated, in which methacrylic acid and ethylene glycol dimethacrylate were used as the functional and cross-linking monomer, respectively, to functionalize the surface of the CdSe quantum dots.[14,15] The fluorescence of these quantum dots, emitted at the wavelength of 605 nm, was quenched due to binding of DNT (Scheme 1) and TNT by the MIP films coating the quantum dots. However, the LOD reached was high, ranging from 0.1 to 0.5 μM, and the chemosensor was applicable only for operation in liquids. In another study, the hierarchically imprinted silica film was pretreated with the 510-nm diameter polystyrene particles to increase its porosity. In effect, LOD of 8.8 nM TNT was reached with the fluorescence quenching of the imprinted silica film at the 235-nm excitation wavelength.[16]

For gas-phase TNT detection, integration of a polysilane recognition MIP film with the waveguide interferometric transducer permitted measurement of the refractive index of the film with LOD of 2.4 ppt TNT.[17] Similarly, an acrylamine film was spin-coated on a quartz crystal resonator (QCR) of a microbalance for the TNT determination. For that, the TNT uptake of ∼150 pg per μg of MIP per hour was measured.[18]

In continuation of our former research on devising and fabricating MIP chemosensors for determination of substances of environmental importance,[19−23] we herein designed and synthesized a new functional monomer of our series of bis(2,2′-bithienyl)methane derivatives, vis. bis(2,2′-bithienyl)-(4-aminophenyl)methane **1** (Scheme 2), for determination of some common NT analytes, such as TNT, TNP, TNB, and DNT. Recognition of these analytes was due to the $\pi-\pi$ interactions of the benzene ring of the NT molecule and that of the phenylamine group of **1**. Furthermore, for the first time, to the best our knowledge, chemical recognition signals were transduced into analytical signals of simultaneous changes of chronoamperometry (CA) cathodic current and piezoelectric microgravimetry (PM) resonant frequency of the MIP films under flow-injection analysis (FIA) conditions.

Scheme 2. Crystal Structure of 1

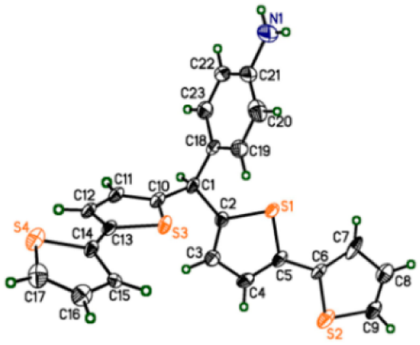

EXPERIMENTAL SECTION

Chemicals. Acetonitrile (ACN), 1,2-dichlorobenzene (DCB), TNB, TNP, DNT, and all chemicals for the synthesis were purchased from Sigma-Aldrich. Tetra-*n*-butylammonium perchlorate, (TBA)ClO_4, was supplied by SACHEM. Hydrochloric acid (HCl) and potassium chloride (KCl) were from Fisher. Toluene and methanol were procured from EMD. TNT was purchased from CHEM Service. The tris([2,2′-bithiophen]-5-yl)methane cross-linking monomer **2** was prepared according to our described procedure.[24] The procedure of synthesis and crystallization of the functional monomer **1** (Scheme 2) was shown in Appendix S1 in Supporting Information.

Instrumentation and Procedures. The ^{1}H NMR spectra were recorded with a broadband dual-channel 400-MHz Varian NMR spectrometer. It featured a highly homogeneous superconducting magnet (9.4 T) and 4 nuclear (1H/9F/13C/31P) probes. The collected spectra were processed using the VNMR Varian software installed on a workstation computer. The 5-mm internal diameter NMR quartz tubes were purchased from Wilmad-LabGlass. Deuterated chloroform exhibiting the 7.24-^{1}H chemical shift was supplied by Cambridge Isotope Laboratories.

The crystal structure of **1** was determined by the Bruker SMART APEX II three-cycle single-crystal diffractometer, equipped with the 16-M pixel charge-couple device (CCD) detectors and the Siemens X-ray sealed tube (Mo Kα radiation, λ = 0.071 nm). Measurements were performed at 100 K. The collected data were processed by the Bruker Suite software.

The UV−vis spectra were recorded with 0.1-nm resolution using the UV-2550 spectrophotometer of Shimadzu Corp. controlled by the UVProbe 2.21 software of the same manufacturer.

Monomer **1** was titrated with each NT, with the fluorescent end point detection, using the Cary Eclipse fluorimeter with accuracy of ±1 nm. A xenon lamp serving as the excitation source was positioned at 90° to the emission detector. The collected emission data were processed by the Scan Application software of the same company.

The recognition MIP films were imaged by atomic force microscopy (AFM) using a MultiMode 8 AFM under control of the Nanoscope V controller of Bruker. The tapping mode was utilized for this imaging with the use of the RTESP probes provided by Bruker. The 0.5 × 0.5 μm^2 film area was analyzed. The films for imaging were deposited on the Au-coated glass slides. The slides were cleaned with acetone, and then dried in an Ar stream prior to film deposition.

The X-ray photoelectron spectroscopy (XPS) spectra were recorded on a PHI 5000 VersaProbe (ULVAC-PHI) scanning ESCA microprobe using monochromatic Al Kα radiation ($h\nu$ = 1486.6 eV). The Casa XPS software was used to evaluate the XPS data. Background was subtracted using the Shirley method, and peaks were fitted with the (Gaussian−Lorentzian)-shaped

dx.doi.org/10.1021/ac4017677 | Anal. Chem. 2013, 85, 8361−8368

profiles. The binding energy (BE) scale was referenced to the C 1s electron peak with BE = 284.6 eV.

The cyclic voltammetry (CV) and DPV measurements were performed by the PARSTAT 2273 computerized electrochemistry system of Princeton Applied Research, equipped with the potentiostat/galvanostat/frequency-response-analyzer and controlled by the PowerSuite software of the same manufacturer. Resolution of the CV potential measurement was ±2 mV. A 1-mm diameter Pt disk, Pt wire, and Ag/AgCl served as the working, auxiliary, and reference electrode, respectively.

The CA and PM experiments were performed under either the FIA or batch analysis conditions using a model EQCM 5610[25] or EQCM 5710 quartz crystal microbalance, respectively, controlled by the EQCM 5710-S2 software, and the EP-20 potentiostat, all of IPC PAS. The resonant frequency change was measured with 0.1-Hz resolution using 14-mm diameter AT-cut plano−plano 10-MHz resonant frequency QCRs with 5-mm diameter and ∼100-nm thick circular Au-film electrodes evaporated over Ti underlayers on both sides of QCRs. However, only one QCR side was wetted by a working solution, and the Au-film electrode of this side was used both as the working electrode and the substrate for deposition of an MIP recognition film.

The NT-extracted MIP-NT film-coated Au-QCRs were examined under FIA conditions. The carrier liquid was pumped at the 20 μL/min flow rate through the EQCM 5610 holder with a model NE-500 syringe pump of New Era Pump Systems. A sample solution of the 200 μL volume was injected with a model 7725i rotary six-port valve of Rheodyne. Analyte samples were dissolved in the solution of the same composition as that of the carrier liquid, i.e., 0.2 M NaCl in water/ACN (1:1, *v*:*v*) for simultaneous CA-PM determination, respectively.[26,27]

Deposition of the NT Template and the MIP-NT Films. The NT films, serving as control films for the XPS characterization, were deposited by drop coating on the Au-coated glass slides from the concentrated NT 1,2-dichloromethane solutions.

The MIP-NT films were deposited on the 6 × 6 mm^2 Au-coated glass slides, and Au-QCRs by potentiodynamic electropolymerization with potentials cycled between 0.50 and 1.25 V versus Ag/AgCl at the scan rate of 50 mV s^{-1}. After three potential cycles, the deposition was stopped and the MIP-NT film washed with acetonitrile to completely remove the supporting electrolyte.

Calculations and Data Fitting. Molecular structure, stoichiometry, the highest occupied molecular orbital (HOMO) and lowest unoccupied molecular orbital (LUMO) energy, as well as values of thermodynamic functions of formation of complexes of **1** with each NT were DFT modeled at the M062X/3-21G* level using the Gaussian 09 software.[28]

RESULTS AND DISCUSSION

Complexation of NT and 1 in Toluene. In view of moderate polarity of both NTs and **1**, a toluene nonpolar solvent was chosen for fluorescence titration. That was because of low electric permittivity (ε = 2.374) and, hence, high solubility of both these compounds in toluene and enhanced intermolecular interactions of NT and **1**. Moreover, its high boiling point (110.6 °C) enables maintaining concentration of both **1** and NT constant all throughout the titration. Then, emission spectra of **1** were recorded by exciting its bis(2,2′-bithienyl)methane moiety at 350 nm. The emission band of **1** during titration with NTs (Figure 1) can be ascribed to fluorescence of its bis(2,2′-bithienyl)methane moiety.[29] After

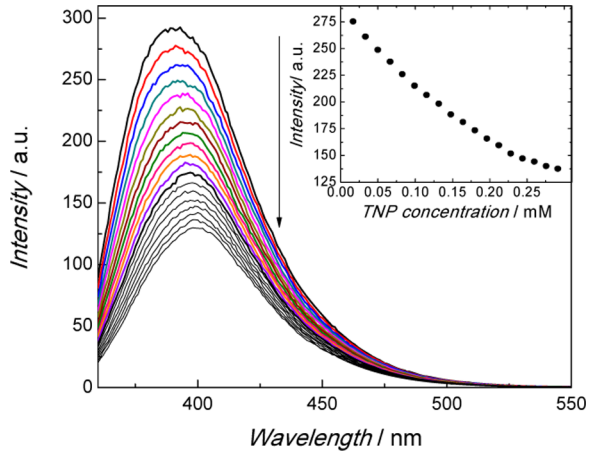

Figure 1. Steady-state fluorescence of **1** quenched by TNP in toluene. Excitation at 350 nm. Initial concentration of **1** was c_1^0 = 0.25 mM, and TNP concentrations were varied in the range 0.017 ≤ c_{NT} ≤ 0.3 mM.

consecutive addition of each NT titrant, the emission intensity of **1** was gradually quenched (Figure 1). That was presumably due to the electron transfer from the photoexcited bis(2,2′-bithienyl)methane moiety of **1** to NT, an electron acceptor (see below). By plotting the emission intensity against concentration of each of the NT titrant (Figure 1 insets and Table S6), we determined stoichiometry of 1:1 for all the **1**−NT complexes. Therefore, the complexation equilibrium of **1** and NT can be expressed, as follows.

$$\mathbf{1} + \mathrm{NT} \rightleftarrows \mathbf{1}\text{−}\mathrm{NT} \quad (1)$$

Then, Benesi−Hildebrand eq 2[30] was applied to calculate stability constant, *K*, values of these complexes.

$$\frac{1}{I - I_0} = \frac{1}{C_{\mathbf{1}}^{\,0} K \Delta\varepsilon_{\mathbf{1}\text{−}\mathrm{NT}} C_{\mathrm{NT}}} + \frac{1}{C_{\mathbf{1}}^{\,0} \Delta\varepsilon_{\mathbf{1}\text{−}\mathrm{NT}}} \quad (2)$$

Symbols I_0 and I represent the fluorescence intensity before and after addition of the NT titrant, respectively. Symbol c_1^0 and c_{NT} stand for the starting concentration of **1** (0.25 mM) and the concentration of the NT titrant, respectively. $\Delta\varepsilon_{1\text{−}NT} = \varepsilon_{1\text{−}NT} - \varepsilon_1 - \varepsilon_{NT}$, where ε_{1-NT}, ε_1, and ε_{NT} is the molar absorptivity of the **1**−NT complex, **1**, and NT, respectively.

Next, by dividing intercepts by slopes of eq 2, we arrived at values of the complex stability constants (Table 1). Apparently, the stability constant of the **1**−TNP complex is the highest, being one-and-a-half times higher than that of the **1**−TNT complex, twice that of the **1**−TNB complex, and over thrice

Table 1. Shift of the CV Anodic Half-Peak Potential, $\Delta E_{pa/2}$, Complex Stability Constant, *K*, and Gibbs Energy Gain, ΔG[a]

NT	$\Delta E_{pa/2}$/mV	K/M^{-1}	ΔG/kJ mol^{-1}
TNP	102	3000	−58.1
TNT	20	2044	−51.8
TNB	29	1596	−48.7
DNT	17	858	−36.4

[a]Due to formation of the 1:1 complexes of **1** and different NTs. Values determined by cyclic voltammetry, from fluorescence quenching, and calculated using the density functional theory (DFT) at the M602X/3-21G* level, respectively.

dx.doi.org/10.1021/ac4017677 | Anal. Chem. 2013, 85, 8361−8368

that of the **1**−DNT complex. Differences in stability of different **1**−NT complexes originate from differences in molecular structures of these complexes, i.e., the presence of different benzene-ring substituents (see below). Moreover, the stability constant of the **1**−TNB complex determined herein was higher than that of the bisporphyrins−TNB complex.[31] The present higher *K* value was due to the use of a low electric permittivity solvent (toluene) rather than a much higher electric permittivity solvent (1% pyridine in methanol) used for the bisporphyrins−TNB complex in ref 31. Conclusively, the solvent nature plays an important role in this complexation.

Molecular Modeling of Structures of the 1−NT Complexes. To determine stoichiometry and optimize structure of the complexes of **1** and the NT analytes, their complexes were DFT modeled at the M062X/3-21G* level (Scheme 3). For that, the M062X density functional method

Scheme 3. Molecular Structure of the 1:1 Complexes of 1 and (a) TNP, (b) TNT, (c) TNB, and (d) DNT, Optimized Using DFT at the M062X/3-21G* Level

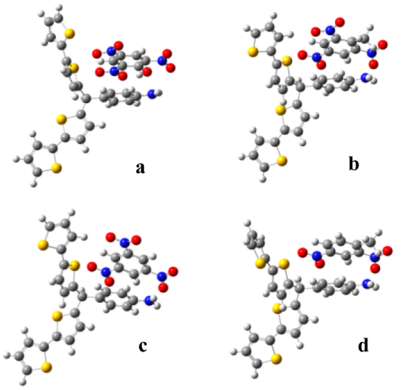

appeared favorable because of its high accuracy in optimization of noncovalent bonds.[32] Expectedly, the $\pi-\pi$ stacking, with a small deflection angle between the NT molecule plane and that of the phenylamine moiety of **1**, bound one molecule of NT with one molecule of **1** in accord with the crystal structure of the complex of 4-(4-aminophenylsulfonyl)aniline and TNB.[33] However, the $\pi-\pi$ stacking distance calculated herein for the structure-optimized complexes of **1** and different NTs were in the range 0.29−0.31 nm. These distances were shorter than that of ∼0.36 nm determined for the complex of 4-(4-aminophenylsulfonyl)aniline and TNB[33] indicating stronger binding between **1** and NT in the former complexes.

Moreover, values of the Gibbs energy gain due to formation of each complex were calculated at the same DFT level. Expectedly, this gain fairly well correlated with the complex stability constant determined by the fluorescence titration (Table 1). However, differences between these gain values are not as large as those between stability constants because of at least two reasons: (i) vacuum rather than a solvent was used as the complexation medium for optimization, and (ii) no steric (only interaction of two complex components) effect was taken into account for optimization of the complex structure. Furthermore, the observed differences in the experimental complex stability constants can roughly be accounted for by concomitant differences in the energy difference between the HOMO and LUMO energy levels of the complexes E_g (Figure S5). First, HOMO of all the complexes is located on the bis(2,2′-bithienyl)methane moiety of **1**. Second, LUMO is located on the NT molecule. Herein, the amine group of **1** is very significant for binding to NTs, so that the excited electron is most likely intermolecularly HOMO-to-LUMO transferred within the complex. Therefore, fluorescence of the bis(2,2′-bithienyl)methane moiety of **1** was quenched in the course of titration of **1** with NTs. Apparently, stability constants are inversely proportional to E_g because the higher the E_g energy gap, the less probable the electron transfer from the photoexcited bis(2,2′-bithienyl)methane moiety of **1** to the LUMO of NTs is (Figure S5).

As an alternative to the **1**−NT complex formation by the $\pi-\pi$ interactions, the complex of **1** and TNB, formed due to hydrogen bonding at the amine-nitro position, was optimized at the same M062X/3-21G* level (Figure S4). However, the hydrogen bonding was not favorable in the latter because of the positive Gibbs energy gain (10.15 kJ/mol) obtained. This gain was positive because the enthalpy decrease due to the hydrogen bond formation was small (−30.15 kJ/mol) compared to the entropy decrease (−135.68 J/mol K).

Cyclic Voltammetry of NTs and 1. CV measurements on the NT analytes and **1** were carried out by using 0.1 M $(TBA)ClO_4$ in ACN/DCB (1:1, *v*:*v*). The same solution conditions were used for the electropolymerization (see Deposition and AFM Characterization of the MIP-NT Films by Electropolymerization section, below). This mixed solvent solution was appropriate for dissolution of both **1** and NT, stable **1**−NT prepolymerization complex formation, and subsequent electropolymerization of this complex.

For all NTs, there was no anodic CV peak in the positive potential range. However, at negative potentials an irreversible cathodic peak appeared for each NT (curves 1−4 in Figure 2).[34] Moreover, cathodic peak potentials were different for each

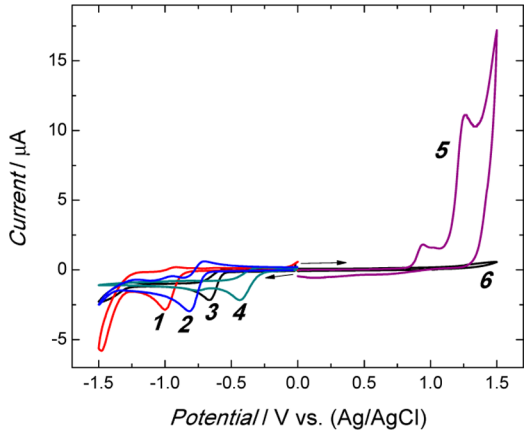

Figure 2. Cyclic voltammograms, recorded at the 1-mm diameter Pt electrode, for 1 mM (1) DNT, (2) TNT, (3) TNB, (4) TNP, (5) **1** in 0.1 M $(TBA)ClO_4$ in ACN/DCB (1:1, *v*:*v*), and (6) a blank supporting electrolyte solution. The potential scan rate was 50 mV s^{-1}.

NT, being equal to −1.00, −0.80, −0.65, and −0.42 V for DNT, TNT, TNB, and TNP, respectively, because of different number of substituents and regioisomerism of substitution of the phenyl ring.[5] For example, DNT has only two nitro (electron-withdrawing) groups compared to those three of TNT. So, the benzene ring of DNT is more negatively charged than that of TNT. In effect, more negative potential is required to reduce DNT. Similarly, TNP has one more electron-withdrawing group (−OH). Therefore, its cathodic peak potential is most positive. Hence, the experimental complex

dx.doi.org/10.1021/ac4017677 | *Anal. Chem.* 2013, 85, 8361−8368

stability constant and the theoretical Gibbs energy gain of the complex formation concomitantly decreased from **1**−TNP to **1**−DNT (Table 1). Because NTs are electron acceptors, the better electron acceptor the NT is, the lower is the potential necessary to reduce it. Hence, the electron is much easier transferred from the bis(2,2′-bithienyl)methane moiety to the TNP molecule than to any other NT molecule (see above).

In contrast, there were two anodic peaks, vis., at 1.00 and 1.25 V, for **1** (curve 5 in Figure 2). They correspond to electro-oxidation of the amine group[35] and the bis(2,2′-bithienyl)-methane moiety[36] of **1**, respectively. By examining electro-oxidation of the former, which leads to formation of a cation radical at the nitrogen atom position, we estimated the ability of **1** to bind to different NTs. For that, we determined shifts of the anodic half-peak potential ($\Delta E_{pa/2}$), recorded after addition of NTs, to reach the concentration of 1 mM, to the solution of 1 mM **1** and 0.1 M (TBA)ClO_4 in ACN/DCB (1:1, *v*:*v*) (Table 1 and Figure S6). The relative shift of the $\Delta E_{pa/2}$ values was consistent with the results of the fluorescence titration, i.e., the $\Delta E_{pa/2}$ value for the **1**−TNP complex was much higher than those for the other were; the $\Delta E_{pa/2}$ value for **1**−DNT was the lowest. In connection with these potential shifts, the more stable the complex, the easier was its electro-oxidation.

Deposition by Electropolymerization and AFM Characterization of the MIP-NT Films. Our DFT calculations, fluorescence titration, and the shifts of the CV anodic half-peak potentials of **1** in the presence of NTs have proven the formation of the **1**−NT prepolymerization complexes in solutions. Next, these complexes were immobilized on the electrode surfaces by potentiodynamic electropolymerization in the NT-templated MIP-NT films. The solutions for electropolymerization were made 0.5 mM in one of the NT analytes, 0.5 mM in **1**, 1.5 mM in **2**, and 0.1 M in (TBA)ClO_4 in ACN/DCB (1:1, *v*:*v*), in order to meet the 1:1 stoichiometry of the **1**−NT complexes. The cross-linking monomer **2** was added in a large excess in order to fix the MIP-NT matrix rigidly. That way the cavity shapes could remain unchanged after template extraction. The presence of the ClO_4^- anions increased conductivity of the MIP-NT film, and the large-size TBA^+ cations contributed to porosity of the films.[37] The anodic peak potential of oxidation of the $-NH_2$ group and that of the bis(2,2′-bithienyl)methane moiety of **1** was shifted toward more positive potentials after the first potential cycle (Figure 3a), and then completely disappeared in subsequent cycles (not shown). This is because each deposited polymer layer played a role of a resistive barrier (Figure 3c). Therefore, the MIP-TNT layers deposited in the course of the next two cycles played the role of the recognition film. That was because no $-NH_2$ group of **1** was electro-oxidized, thus favoring the subsequent NT recognition. Similarly, all other MIP-NT films were deposited on the Pt electrodes from their respective solutions.

Furthermore, the decrease of the resonant frequency observed after each potential cycle indicated that the more resistive the MIP-TNT film, the smaller mass of MIP was deposited (Figure 3b).

Surface of the MIP-TNT film was imaged by AFM. The polymer film was composed of the 20−30-nm diameter grains (Figure 4). The determined film roughness of 1.3 ± 0.1 nm indicated formation of a relatively smooth film.

Extraction of the NT Templates from the MIP-NT Film. By analogy to the previously reported TNT template extraction with ethanol,[38] a mixed solution of MeOH/ACN (1:1, *v*:*v*) was used herein for the NT template extraction under vigorous

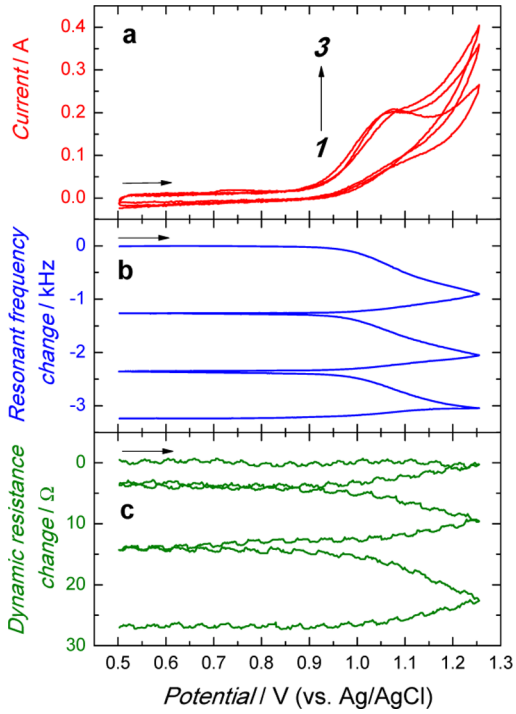

Figure 3. Simultaneously recorded curves of (a) potentiodynamic electropolymerization, (b) resonant frequency change, and (c) dynamic resistance change for deposition of the MIP-TNP film on the Au-QCR from 0.5 mM TNT, 0.5 mM **1**, 1.5 mM **2**, and 0.1 M (TBA)ClO_4 in ACN/DCB (1:1, *v*:*v*). Potential cycle numbers are indicated at curves. The potential scan rate was 50 mV s^{-1}.

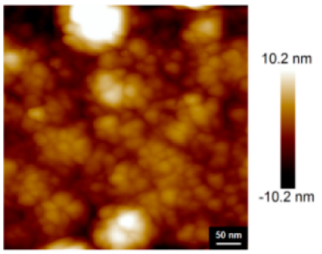

Figure 4. Atomic force microscopy (AFM) image of the MIP-TNT film deposited by 3 potential cycles on the Au-coated glass slide, measured at the 0.5 × 0.5 μm^2 surface area.

magnetic stirring conditions. This solvent selection followed from high affinity of the −OH group of methanol to the $-NO_2$ group of the NT template on the one hand and high solubility of the template in ACN on the other.

Because the binding energy of the N 1s electron of the $-NO_2$ group of NT is different from that of the $-NH_2$ group of **1**, the XPS measurements are useful to confirm the template binding and then completeness of its extraction. Therefore, first, the XPS high resolved spectrum of a drop-coated TNT film was recorded as a reference. There is a well-developed strong peak at ∼406.2 eV (Figure 5a) for the N 1s electron of the $-NO_2$ group.[39] Moreover, the XPS spectrum of a control NIP film was recorded to distinguish the binding energy of the N 1s electron of the $-NH_2$ group from that of the $-NO_2$ groups (Figure 5b). In fact, two peaks seen at 399.8 and 401.8 eV correspond to the $-NH_2$ and $-NH_3^+$ group, respectively, of the functional monomer **1**.[20] Herein, the peak for the $-NH_3^+$ group emerged due to electro-oxidation of the $-NH_2$ group

dx.doi.org/10.1021/ac4017677 | *Anal. Chem.* 2013, 85, 8361−8368

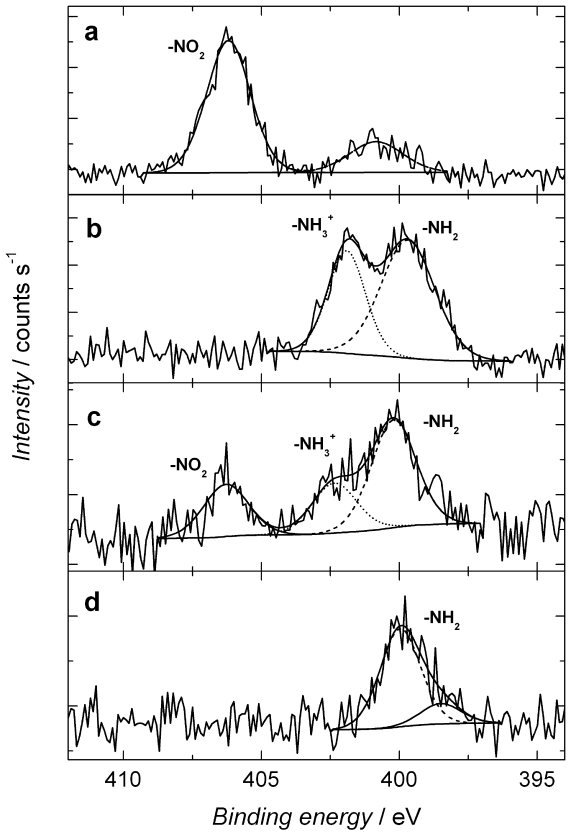

Figure 5. X-ray photoelectron spectroscopy (XPS) spectra of the N 1s electron for (a) the drop-coated TNT film, (b) the NIP film as well as the MIP-TNT film deposited, by electropolymerization, on the Au-coated glass slides, (c) before and (d) after TNT extraction with MeOH/ACN (1:1, *v*:*v*). Assignments of the nitrogen atoms for deconvoluted peaks are indicated at spectra.

during electropolymerization. Expectedly, all three N 1s signals of the $-NO_2$, $-NH_2$, and $-NH_3^+$ group appeared in the XPS spectrum of the TNP-templated MIP-TNT film (Figure 5c). After the TNP extraction, however, the N 1s peak of $-NO_2$ disappeared thus confirming completeness of the extraction (Figure 5d). Besides, $-NH_3^+$ was deprotonated to $-NH_2$ during extraction in connection with disappearance of the 401.8 eV peak (Figure 5d).

Moreover, the cathodic peak potential of the TNP electropolymerization was used for verification of the extraction completeness. By way of example, the DPV curve for 2 mM TNP in 0.1 M NaCl was recorded in the range −0.1 to −0.6 V in a control experiment with the peak potential of ∼−0.4 V (curve 1 in Figure S7).[40] Next, the DPV curve for the TNP-templated MIP-TNP film in 0.1 M NaCl was recorded. In effect, the TNP peak was clearly seen at ∼-0.35 V (curve 2 in Figure S7). Herein, a ∼0.05 V positive potential shift of the peak of the TNP-templated MIP-TNP film against that of TNP in solution (curve 1 in Figure S7) may be due to complexation of **1** and TNP in the former. After TNP extraction from the film, the peak disappeared (curve 3 in Figure S7) indicating that TNP was completely extracted, indeed.

Selective Determination of NTs by Simultaneous Chronoamperometry and Piezoelectric Microgravimetry under Flow-Injection Analysis Condition. From the different cathodic CV peak potential of each NT electroreduction (curves 1−4 in Figure 2a), we could selectively determine each NT under FIA conditions with chronoamperometry by applying constant potential of −0.40, −0.65, −0.80, and −1.00 V for TNP, TNB, TNT, and DNT, respectively, and measuring cathodic current versus time. However, cathodic CV peak potential for reduction of bis(2,2′-bithienyl)methane is ∼−1.00 V.[41] Therefore, chronoamperometry could not be applied for the DNT determination because of electrochemical decomposition of the MIP film. Simultaneously, the resonant frequency changes were recorded when NT molecules entered and left cavities of the NT-extracted MIP-NT film increasing and decreasing its mass, respectively.

Expectedly, both cathodic current and resonant frequency, recorded using the MIP-TNT film-coated Au-QCR, changed producing peaks after each injection of 0.2 M NaCl solution of TNT of different concentration indicating reversible binding of TNT with cavities of the MIP-TNT film (Figure 6).

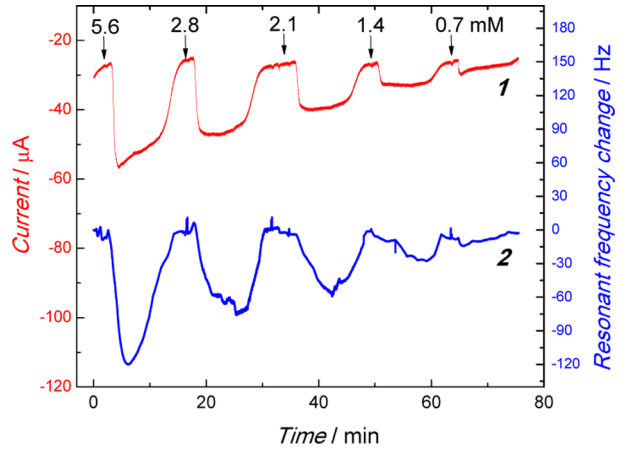

Figure 6. Simultaneous change, at −0.80 V vs Ag/AgCl, of (1) cathodic current and (2) resonant frequency with time during injection of 0.2 M NaCl in water/ACN (1:1, *v*:*v*) solutions of TNT of different concentrations (final TNT concentrations in solution are indicated with numbers at each step) under FIA conditions for the TNT-extracted MIP-TNT film-coated Au-QCR.

For CA determination of TNT, the linear dynamic concentration range was 0.7−5.6 mM obeying the linear regression equation of $I_c/\mu A$ = 2.08 (±0.67) − 5.65 (±0.20) c_{TNT}/mM with the correlation coefficient of 0.99 (curve 2 in Figure S9a). At the signal-to-noise ratio, S/N = 3, detectability of the CA chemosensor was LOD = 0.62 mM, with the 5.65 (±0.20) μA/mM sensitivity. Herein, the CA cathodic current recorded at the MIP-coated Au-QCR was 7.5-times that at the bare Au-QCR for the injected solution of 5.6 mM TNT (Figure S8). That was because, after TNT injection, it accumulated in the MIP-film making its concentration in the electrode vicinity much higher than that in the bulk solution. Similarly, LOD of the CA chemosensors for TNP and TNB were 0.69 and 0.27 mM (Table 2). However, sensitivities of all three CA chemosensor were similar, i.e., equal to 7.34 (±0.81), 5.65 (±0.20), and 6.33 (±0.29) μA/mM for TNP, TNT, and TNB, respectively (Figure S9a). That might be because the cathodic current is not only controlled by the NT accumulation in the MIP-NT film, but also by the applied potential and diffusion coefficient of each NT.

For PM determination of TNT, the linear dynamic concentration range was 0.7−5.6 mM TNT with the linear regression equation of Δf/Hz = 0.37 (±0.38) − 21.41 (±1.11)

dx.doi.org/10.1021/ac4017677 | *Anal. Chem.* 2013, 85, 8361−8368

Table 2. Detectability (LOD) and Selectivity of the MIP-NT Chemosensors[a]

	LOD/mM		selectivity	
chemosensor	CA	PM	CA	PM
MIP-TNP	0.69	0.02	2.6 (to TNT)	4.8 (to TNT)
MIP-TNT	0.62	0.07	2.1 (to TNP)	3.1 (to TNP)
MIP-TNB	0.27	0.15	2.4 (to TNT)	2.7 (to TNT)
MIP-DNT		0.76		3.0 (to TNB)

[a]Determined for the 0.2 M NaCl solutions of water/ACN (1:1, *v*:*v*), by injecting analyte and interference solutions of different concentrations.

c_{TNT}/mM and the correlation coefficient of 0.99 (curve 2 in Figure S9b). At S/N = 3, the TNT detectability of the PM chemosensor was LOD = 70 μM, with the 21.41 (±1.11) Hz/mM sensitivity. Similarly, the calibration plots for the 0.2 M NaCl solutions of TNT, TNB, or DNT, constructed using their corresponding MIP-NT recognition films, are shown in Figure S9b and analytical parameters determined summarized in Table 2. Among them, the sensitivity of the PM-chemosensor for DNT is the lowest. This is because weaker binding of **1** and DNT results in accumulation of a smaller amount of DNT in the MIP-DNT film. Therefore, a higher DNT concentration (higher LOD) was necessary to generate the measurable signal. Generally, LOD of the PM chemosensor is by one order of magnitude lower than that of the CA chemosensor.

For determination of the imprinting factor, a NIP film-coated Au-QCR was prepared as a control for TNB determination by PM (curve 5 in Figure S9b). The linear dynamic concentration range was 0.7−5.6 mM obeying the linear regression equation of Δf/Hz = 0.63 (±0.11) − 1.92 (±0.32)c_{TNT}/mM with the correlation coefficient of 0.90. By dividing the slope of the calibration curve for the MIP-TNB film by that for the NIP film, we arrived to the appreciable imprinting factor of 4.8.

Moreover, selectivity of the NT chemosensors was determined by cross-imprinting. That is, the template of one MIP-NT chemosensor was used as an interference of other chemosensors. In our experiments, selectivity of each MIP-NT chemosensor was examined with respect to two different transducers, and the determined selectivity values are compiled in Table 2. The MIP-TNP chemosensor appeared to be the most selective because of its strongest analyte binding. Moreover, selectivity of these chemosensors is controlled by the method of transduction, i.e., PM-chemosensors are more selective than CA chemosensors.

CONCLUSIONS

We developed a one-pot procedure of synthesis of a new functional monomer, bis(2,2′-bithienyl)-(4-aminophenyl)-methane **1**, for selective binding of nitroaromatic explosives by $\pi-\pi$ stacking. The bis(2,2′-bithienyl)methane moiety of **1** revealed several advantages with respect to sensing of NTs. These included playing a fluorophore role for the fluorescence titration, decreasing polarity of **1** in order to make it soluble in an organic solvent of low polarity, and enabling **1** to electropolymerize to result in an MIP-NT film deposited on the electrode surface. Besides, the phenylamine group of **1** was an appreciable $\pi-\pi$ recognizing site of NT, as demonstrated by the fluorescence titration, DFT molecular modeling, and the CV anodic half-peak potential shift of the phenylamine moiety electro-oxidation. The M062X method appeared suitable for modeling the $\pi-\pi$ interactions, which well correlated with the experimental complexation data. Moreover, the modeling results helped to understand more deeply the nature of the $\pi-\pi$ stacking of the phenylamine moiety of **1** and NT at the 1:1 stoichiometry as well as the fluorescence quenching of the bis(2,2′-bithienyl)methane moiety of **1** by the intermolecular electron transfer.

Potentiodynamic electropolymerization is a superior way of the complex transfer from the solution onto the electrode surface. In effect thin, well-adhesive, and homogeneous polymer films are deposited. Besides, XPS has proven to serve as an advanced method to directly confirm the presence of the NT template in the MIP-NT films and its subsequent extraction by monitoring N 1s electron binding energy peaks of the $-NO_2$ groups of NTs. The DPV measurements confirmed these results.

For sensing application, the first ever simultaneous measurement herein of the change of the CA cathodic current and PM resonant frequency opened up a new reliable and sensitive avenue to dual selective determination of the NT explosives. The LOD values of the fabricated chemosensors ranged between 0.27 to 0.69 and 0.02 to 0.76 μM for the CA and PM determination, respectively, with detectability of the PM chemosensor lower than that of the CA chemosensor. Because of their low detectability, both chemosensors are well applicable to determine nitroaromatic explosives in real samples. Moreover, selectivity studies, performed by cross-imprinting of interferences structurally similar to the target NTs, revealed that the chemosensors were prevailingly sensitive to the analytes used for templating.

ASSOCIATED CONTENT

Supporting Information

Preparation of bis(2,2′-bithienyl)-(4-aminophenyl)methane **1**; ^{1}H NMR, mass, UV−vis, and fluorescence spectra of **1**; CV and DPV data; tables of crystal structure details. This material is available free of charge via the Internet at http://pubs.acs.org.

AUTHOR INFORMATION

Corresponding Author

*E-mail: francis.dsouza@unt.edu (F.D.), wkutner@ichf.edu.pl (W.K.) Phone: +940-369-8832 (F.D.), +48 22 343 3217 (W.K.). Fax: 940 565 4318 (F.D.), +(48 22) 343 3333 (W.K.).

Notes

The authors declare no competing financial interest.

ACKNOWLEDGMENTS

The present research was financially supported by the Foundation for Polish Science (Project MPD/2009/1/styp19) to T.-P.H. and (Project MPD/2009/1/styp15) to M.S., the European Regional Development Fund (Project ERDF, No. POIG.01.01.02-00-008/08 2007-2013) to W.K., and the U.S. National Science Foundation (Grant 1110942) to F.D.

REFERENCES

(1) Lesage, S.; Jackson, R. E., *Groundwater Contamination and Analysis at Hazardous Waste Sites*; Marcel Dekker, Inc.: New York, 1992.

(2) Patnaik, P. In *A Comprehensive Guide to the Hazardous Properties of Chemical Substances*, 3rd ed.; John Wiley & Sons: New York, 2007; pp 691−702.

(3) Mantha, R.; Biswas, N.; Taylor, K. E.; Bewtr, J. K. *Water Environ. Res.* **2002**, *74*, 280−287.

(4) Cruz-Uribe, O.; Rorrer, G. L. *Biotechnol. Bioeng.* **2005**, *93*, 401−412.
(5) Toal, S. J.; Trogler, W. C. *J. Mater. Chem.* **2006**, *16*, 2871−2883.
(6) Salinas, Y.; Martınez-Manez, R.; Marcos, M. D.; Sancenon, F.; Costero, A. M.; Parra, M.; Gil, S. *Chem. Soc. Rev.* **2012**, *41*, 1261−1296.
(7) Wang, J. *Electroanalysis* **2007**, *19*, 415−423.
(8) Haupt, K. *Analyst* **2001**, *126*, 747−756.
(9) McCluskey, A.; Holdsworth, C. I.; Bowyer, M. C. *Org. Biomol. Chem.* **2007**, *5*, 3233−3244.
(10) Sharma, P. S.; D'Souza, F.; Kutner, W. In *Portable Chemical Sensors—Weapons Against Bioterrorism, NATO Science for Peace and Security Series A: Chemistry and Biology*; Nikolelis, D. P., Ed.; Springer: Berlin, 2012; pp 63−94.
(11) Sharma, P. S.; D'Souza, F.; Kutner, W. *Trends Anal. Chem.* **2012**, *34*, 59−77.
(12) Apodaca, D. C.; Pernites, R. B.; Mundo, F. R. D.; Advincula, R. C. *Langmuir* **2011**, *27*, 6768−6779.
(13) Nie, D.; Jiang, D.; Zhang, D.; Liang, Y.; Xue, Y.; Zhou, T.; Jin, L.; Shi, G. *Sens. Actuators, B* **2011**, *156*, 43−49.
(14) Stringer, R. C.; Gangopadhyay, S.; Grant, S. A. *Anal. Chem.* **2010**, *82*, 4015−4019.
(15) Stringer, R. C.; Gangopadhyay, S.; Grant, S. A. *Anal. Chim. Acta* **2011**, *703*, 239−244.
(16) Zhu, W.; Tao, S.; Tao, C.-a.; Li, W.; Lin, C.; Li, M.; Wen, Y.; Li, G. *Langmuir* **2011**, *27*, 8451−8457.
(17) Edmiston, P. L.; Campbell, D. P.; Gottfried, D. S.; Baughman, J.; Timmers, M. M. *Sens. Actuators, B* **2010**, *143*, 574−582.
(18) Bunte, G.; Hurttlen, J.; Pontius, H.; Hartlieb, K.; Krause, H. *Anal. Chim. Acta* **2007**, *591*, 49−56.
(19) Pietrzyk, A.; Kutner, W.; Chitta, R.; Zandler, M. E.; D'Souza, F.; Sannicolo, F.; Mussini, P. R. *Anal. Chem.* **2009**, *81*, 10061−10070.
(20) Pietrzyk, A.; Suriyanarayanan, S.; Kutner, W.; Chitta, R.; D'Souza, F. *Anal. Chem.* **2009**, *81*, 2633−2643.
(21) Pietrzyk, A.; Suriyanarayanan, S.; Kutner, W.; Maligaspe, E.; Zandler, M. E.; D'Souza, F. *Bioelectrochemistry* **2010**, *80*, 62−72.
(22) Pietrzyk, A.; Suriyanarayanan, S.; Kutner, W.; Chitta, R.; Zandler, M. E.; D'Souza, F. *Biosens. Bioelectron.* **2010**, *25*, 2522−2529.
(23) Huynh, T.-P.; Pietrzyk-Le, A.; KC, C. B.; Noworyta, K.; Sobczak, J. W.; Sharma, P. S.; D'Souza, F.; Kutner, W. *Biosens. Bioelectron.* **2013**, *41*, 634−641.
(24) Huynh, T.-P.; KC, C. B.; Lisowski, W.; D'Souza, F.; Kutner, W. *Bioelectrochemistry* **2012**, DOI: 10.1016/j.bioelechem.2012.07.003.
(25) Kochman, A.; Krupka, A.; Grissbach, J.; Kutner, W.; Gniewinska, B.; Nafalski, L. *Electroanalysis* **2006**, *18*, 2168−2173.
(26) Toth, K.; Stulik, K.; Kutner, W.; Feher, Z.; Lindner, E. *Pure Appl. Chem.* **2004**, *76*, 1119−1138.
(27) Buck, R. P.; Lindner, E.; Kutner, W.; Inzelt, G. *Pure Appl. Chem.* **2004**, *76*, 1139−1160.
(28) Frisch, M. J.; et al. *Gaussian09*; Gaussian, Inc.: Wallingford, CT, 2009.
(29) Finden, J.; Kunz, T. K.; Branda, N. R.; Wolf, M. O. *Adv. Mater.* **2008**, *20*, 1998−2002.
(30) Atwood, J. L.; Davies, J. E. D.; Macnicol, D. D.; Vogtle, F. In *Comprehensive Supramolecular Chemistry*, 1st ed.; Davies, J. E. D., Ripmeester, J. A., Eds.; Pergamon: Oxford, 1999; Vol. *8*, pp 425−444.
(31) Jeyakumar, D.; Krishnan, V. *Spectrochim. Acta, Part A* **1992**, *48*, 1671−1682.
(32) Hohenstein, E. G.; Chill, S. T.; Sherrill, C. D. *J. Chem. Theory Comput.* **2008**, *4*, 1996−2000.
(33) Smith, G.; Wermuth, U. D. *Acta Crystallogr., Sect. E* **2012**, *68*, 494.
(34) Kemula, W.; Krygowski, T. M. In *Encyclopedia of Electrochemistry of the Elements*; Bard, A. J., Lund, H., Eds.; Marcel Dekker: New York, 1979; Vol. *13*, pp 78−130.
(35) Jannakoudakis, A. D.; Jannakoudakis, P. D.; Pagalos, N.; Theodoridou, E. *Electrochim. Acta* **1992**, *38*, 1559−1566.
(36) Heinze, J.; Frontana-Uribe, B. A.; Ludwigs, S. *Chem. Rev* **2010**, *110*, 4724−4771.
(37) Roncali, J. *Chem. Rev.* **1992**, *92*, 711−738.
(38) Bianchi, F.; Giannetto, M.; Mori, G.; D'Agostino, G.; Careri, M.; Mangia, A. *Anal. Bioanal. Chem.* **2012**, *403*, 2411−2418.
(39) Beamson, G.; Briggs, D. *High Resolution XPS of Organic Polymers, the Scienta ESCA 300 Database*; John Wiley & Sons: Chichester, UK, 1992; pp 206−207.
(40) Lu, X.; Quan, Y.; Xue, Z.; Wu, B.; Qi, H.; Liu, D. *Colloid Surf., B* **2011**, *88*, 396−401.
(41) Levi, M. D.; Aurbach, D. *J. Power Sources* **2008**, *180*, 902−908.